Development and Upgrade of a Laser Cooling and Trapping System of Ultracold Potassium Atoms

A thesis submitted in partial fulfillment of the requirement
for the degree of Bachelor of Science with Honors in
Physics from the College of William and Mary in Virginia,

by
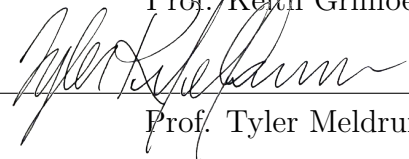
Bennett Atwater

Accepted for Honors

_____

Advisor: Prof. Seth Aubin

_____

Prof. Keith Griffioen

_____

Prof. Tyler Meldrum

Williamsburg, Virginia
May 8, 2020

Contents

Acknowledgments

I would like to thank Seth Aubin for his personal oversight of my project as well as overall support. I would like to thank Andrew Rotunno for his patience, advice, and guidance during my time in lab. As the graduate student on-call most days I was in lab, he withstood the most pestering questions and frustrating requests with grace and graciousness. I would like to thank Will Henninger for his help machining and advising the creation of many of the parts utilized for the project. Finally, I would like to thank Shuangli Du and Doug Beringer for providing their personal support during this process.

List of Figures

vi

Abstract

This thesis describes work to improve the apparatus that cools and loads potassium atoms onto the atom chip. This work consists of two main thrusts: a laser trap translator to help cool and load atoms onto the atom chip and a temperature stabilization system for the lasers that are used to laser cool potassium atoms. The current iteration of the beam translator has the ability to vertically translate a beam ± 4.5 mm relative to its incident height. The translator has been shown to not alter the spatial profile of the beam through interference or obstruction. The translator's rotation has been adjusted to minimize atomic heating once the translator is integrated for use in optical atomic trapping. The translator has been installed on the apparatus but has not yet been tested with ultracold atoms. Furthermore, a feedback system was designed for climate-managing the potassium cooling lasers utilized in the Aubin lab's ultracold apparatus.

Chapter 1

Introduction

Since the late 20th century, ultracold atomic physics has presented an unparalleled platform for the study of atomic and molecular interactions [1]. Stemming from preliminary work on laser cooling by S. Chu and others in the late 1980s, the ability to probe fundamental physical properties in a near-absolute-zero, thermally isolated environment has generated incredible breakthroughs in our understanding of quantum phenomenon as well as exciting new frontiers such as quantum computing [2]. More specifically, the development of ultracold quantum gases has introduced a level of unparalleled control of atoms. From the assembly of molecules via the manipulation of Feshbach resonances to the separation of atomic spin states via spin-specific trapping, the continued study of ultracold systems promises to unlock near limitless possibilities for quantum control [15]. These longer term and ambitious quantum control objectives tie in directly with the goal of this project: upgrading the experimental capabilities of the Aubin Lab's current apparatus to incorporate ultracold potassium atoms.

1.1 The Goal of the Experiment/Research

1.1.1 The Benefits of Potassium

At present, the Aubin lab utilizes rubidium-87 for conducting experiments on the AC Zeeman effect. These experiments focus on the manipulation of atoms via the application of spin-specific microwave potentials [3]. Such a capability is critical for developing spin-dependent trapped atom interferometry as well as logic gates for quantum computing [4]. However, the relatively large hyperfine splitting associated with the ^{87}Rb ground levels ($\approx$ 6.8 GHz) has presented engineering challenges in developing a microwave atom chip capable of producing a satisfactory AC Zeeman trap. In contrast, potassium isotopes have much smaller hyperfine splittings: ^{41}K at 254 MHz, ^{39}K at 462 MHz, and ^{40}K at 1.285 GHz. These smaller, hyperfine splittings require much lower RF frequencies, which also couple much more efficiently to the group's existing atom chip, thus enabling possible trapping experiments in the near term. Furthermore, while ^{87}Rb has few useful magnetic Feshbach resonances at low field, potassium has many promising homonuclear as well as heteronuclear K-Rb resonances in this range. These magnetic Feshbach resonances allow for the tuning of the collisional cross-section for the association of atoms into weakly bound molecules. The Feshbach resonances of interest include ^{41}K at 51 G and ^{41}K-^{87}Rb at 35 G and 79 G [5, 6].

1.1.2 The Problem With Potassium

While the assimilation in 2012-2018 of ^{41}K into the preexisting apparatus presented itself as a seemingly straightforward task, initial attempts at incorporating potassium have met limited success once the atoms are loaded into the group's micro-magnetic atom chip trap. Currently, it is believed that multi-atomic potassium-potassium and potassium-rubidium collisions have made the current apparatus unsatisfactory for

consistent, low-temperature trapping. As a result, the apparatus must be updated, and new components must be implemented, in order to accommodate these unforeseen complications.

1.1.3 A Possible Solution: a Translating Hybrid Trap

Other groups have successfully cooled potassium to Bose-Einstein condensation by sympathetic cooling with rubidium and by direct evaporation, but these efforts have utilized large scale macroscopic traps, not an atom chip micromagnetic trap [13, 5]. There is one exception: an atom chip experiment destined for the International Space Station has succeeded in cooling a very small sample of ^{41}K to BEC [14]. Furthermore, in the Aubin Lab, sympathetic cooling of potassium with rubidium has worked in their macroscopic magnetic trap.
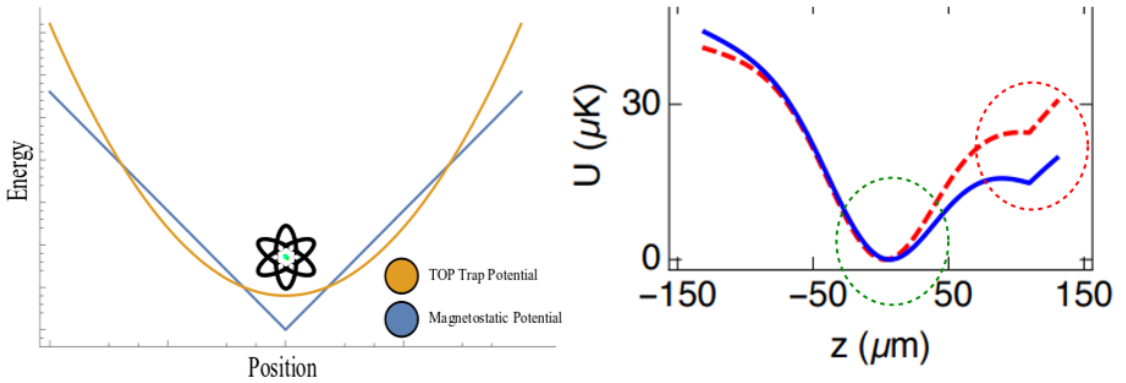
Figure 1.1: Two possible trap potentials. Left: TOP Trap potential. The constant motion of the magnetic field inhibits the atoms within from reaching an energetic minimum and magnetic field zero. This results in the inability of the atoms to spin-flip. Right: Hybrid Trap Potential. Creating an optical offset to the magnetic trap inhibits the atoms within from spin flipping. The red circle marks the energetic minimum of the magnetic trap while the green marks that of the offset optical dipole trap. Right figure taken from reference [11].

A possible solution to the current bottleneck is for the Aubin Lab to do most, or all, of the sympathetic cooling off-chip in a hybrid optical-magnetic trap. This type

of trap has shown itself to be capable of efficiently achieving BEC in potassium [11]. As shown in Figure 1.1-right, this trap combines a quadrupole magnetic trap with an optical dipole trap, such that the optical trap minimum and combined trap minimum are slightly offset from the magnetic trap minimum. This geometric configuration ensures that ultracold atoms at the bottom of the trap cannot undergo a spin-flip by passing through a a magnetic null (i.e. the magnetic trap minimum). Unfortunately, the hybrid optical-magnetic trap must be at least a few millimeters away from the atom chip since the initial cold atom cloud has a radius of this size. Furthermore, once the atoms have been cooled to a BEC, they then must be moved 100 μm from the atom chip to perform experiments.

These dual position requirements can be met via a translating trap. The atoms will be cooled in the hybrid optical-magnetic trap at a distance of about 7 mm from the atom chip. Once sufficiently cooled, the ultracold atom cloud will be substantially smaller (100 μm radius), so the trap can be translated to a distance of 100 μm from the atom chip for experiments. While translating a magnetic trap can be done by adjusting relative currents in magnetic coils, translating an optical dipole trap requires careful translation of the laser beams that form the trap.

1.1.4 Initial Work and Planning

Beginning in the Summer of 2019, the Aubin lab has been working to design a laser beam translator to translate its optical dipole trap. The goal for this device is relatively simple: to create some means of controlled, programmable, 1D, vertical translation for two incident laser beams without altering the beams' spatial profiles. Making use of Snell's law, it was hypothesized that these requirements might be met by sending the beam through a glass window allowed to rotate via an axis perpendicular to the plane of incidence (see Fig. 2.2). This thesis describes work to construct, test,

and implement this rotation stage-based beam translator.

On top of the need for a new, translatable trap, the potassium cooling system also suffers from a technical problem. The cooling lasers for potassium are not stable enough to provide uninterrupted cooling for multiple hours without human intervention. This instability is due to drift in the local room temperature in the vicinity of the potassium lasers. As a second upgrade to the ultracold apparatus, we aimed to design a PID feedback system for thermally controlling the housing for two of the ultracold apparatus's lasers. These lasers are extremely susceptible not only to output wavelength shifts due to temperature but also to the accumulation of water vapor. Both of these issues introduce noise during data collection and reduce the time-frame in which experiments may be performed. By introducing a thermal control system, both of these problems can be minimized if not erased.

1.2   Structure of Thesis

The main results of this thesis are the development of the dipole trap translation system based on a rotating glass plate and the construction of a thermal control circuit for stabilizing the temperature of a laser enclosure. Unfortunately, much of the research was either stopped or considerably slowed down by the COVID-19 pandemic for March-April 2020, thus limiting results that were close to being achieved.

The structure of this thesis is the following. Chapter 2 reviews basic atom trapping methods and the theory for translating an optical dipole trap with a rotating glass plate. Chapter 3 presents the experimental work performed to develop a glass plate with a programmable rotation angle. Chapter 4 presents the development of a thermal controller based on PID feedback. Finally, Chapter 5 concludes by summarizing the results and providing an outlook for future work.

Chapter 2

Optical Dipole Trap Translation Theory

2.1 Basic Cold Atom Traps

Key to the recent success of ultracold atomic physics as a field has been the discovery and design of atomic traps for cooling and confining neutral atoms. Three primary categories of these traps have become ubiquitous to ultracold experiment: radiation pressure traps, magnetic traps, and optical dipole traps [7].

2.1.1 Radiation-Pressure Traps

Firstly, radiation-pressure traps rely on the Doppler effect. Light, whose wavelength is tuned slightly above resonance, is targeted at the atoms to be trapped. The atoms, when moving opposite to the light's direction of propagation, experience this light as having a lower wavelength which shifts the detuned light near-resonance. Upon absorption, these atoms experience a kick opposite to their motion due to conservation of momentum and are slowed. Over time, this leads to an overall decrease in kinetic energy of the system as the moving atoms are repeatedly kicked to lower velocities [10]. Using radiation-pressure traps, atomic physicists have been able to repeatably study systems in the 10 μK range. A prime example of a radiation-pressure trap is

the magneto-optical trap, i.e. MOT, first developed by S. Chu and co-workers in 1987 [12]. The MOT is the laser cooling workhorse of cold atom labs and is the starting point for generating a Bose-Einstein Condensate (BEC).

2.1.2 Magnetic Traps

Magnetic traps are conservative trapping potentials with typical depth in the μK to mK range. The interaction of an atom's magnetic moment with a magnetic field generates a potential that can trap the atom. Typically, these traps confine atoms with temperatures in the nK to several 100 μK range [9]. Applying a magnetic field to a system of atoms will cause the atoms' magnetic moments to align with or against the external field depending on their internal structure. For atoms which align with the field, these atoms will congregate to areas where the incident magnetic field is more intense: these atoms act as strong field seekers. For atoms which align against the field, the opposite is true: these atoms act as weak field seekers. The potential energy of an atom in a magnetic field is determined by the Zeeman effect and the corresponding Zeeman interaction Hamiltonian:

$$\Delta E = -\vec{\mu} \cdot \vec{B} \tag{2.1}$$

where $\vec{\mu}$ is the magnetic moment of the atom, and $\vec{B}$ is the magnetic field of the trap. The neutral atoms migrate to areas where this energy shift provides an energy minimum leading to trapping.

2.1.3 Optical Dipole Traps

Finally, optical dipole traps utilize neutral atoms' electric dipole moments to enable trapping. While relatively complex in derivation, the key to optical dipole trapping comes from the formula for the trapping potential (conservative):

$$U_{dip}(r) = \frac{3\pi c^2}{2\omega_o^3} \frac{\Gamma}{\Delta} I(r) \tag{2.2}$$

where c is the speed of light, Γ is the spontaneous emission rate for the optical transition (i.e. lifetime of the excited state), Δ is the difference between the optical transition frequency ω_0 and the dipole laser frequency ω ($\Delta = \omega - \omega_0$), and $I(r)$ is the intensity profile of the dipole laser [7]. By ensuring that our laser frequency is less than but close to the resonant frequency (i.e. red-detuned), our potential becomes negative and fairly appreciable in magnitude. Combine this with a large beam intensity and this highly negative potential becomes a respectable potential well in which to trap our atoms. Dipole traps typically have depths in the range of 10-100 μK. They are also relatively easy to make: a red-detuned focused laser produces a trap at the focus; sometimes two lasers are focused are overlapped to produce a tighter trap.

2.1.4 Hybrid Optical-Magnetic Trap

The hybrid optical-magnetic trap consists of a quadrupole magnetic trap and an optical dipole. This hybrid trap combines the efficient evaporative cooling of a quadrupole trap with the ability of a dipole trap to provide low-heating confinement for any spin state. The quadrupole trap is generated by two high current coils in anti-Helmholtz configuration while the dipole trap is formed at the focus of a red-detuned laser. Critically, this focus is slightly off-center from the trap minimum of the quadrupole, as shown in Figure 1.1(right): cold atoms that accumulate at the bottom of the trap (during evaporative cooling) are funneled into the dipole trap, while largely avoiding the spin-flipping region of zero magnetic field at the quadrupole minimum. Once the atoms are sufficiently cold, all atoms are contained within the laser dipole trap so the quadrupole trap can be turned off.

2.1.5 Dipole Trap Translation Considerations

In the case of the hybrid optical-magnetic trap planned in the Aubin Lab, once the atoms have been cooled to ultracold temperatures in the dipole trap ($\sim 1\ \mu$K), they must be translated about 5-8 mm to the atom chip. In other words, the dipole trap beams must be physically translated while maintaining a proper focus. Importantly, the translation must be smooth, without vibrations, and automated (via a TTL trigger).
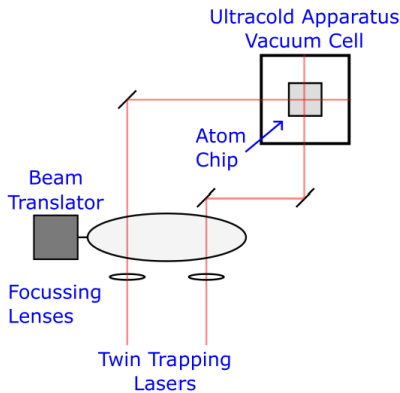
Figure 2.1: Bird's-Eye view of the ultracold apparatus. Two laser beams focused into the center of the ultracold apparatus serve as the optical portion of a hybrid optical trap. This allows for vertical tuning of the position of the atoms within the trap during experiments.

A simple translation device is a mirror placed between the focusing lens and the trap: by tilting the mirror, the laser focus is translated. Conveniently, with a long focal distance the mirror only needs to be tilted a small amount. Unfortunately, any vibration on the mirror during the tilting will result in amplified position jitter at the focus, thus leading to heating of the atoms.

A lower vibration alternative is to use a tilted glass window (see Fig. 2.1). If the windows sides are truly parallel, then the output beam will experience a true translation and will be parallel to the input beam, as shown in Figure 2.2. Furthermore, any up-down or side-to-side vibration will not affect the laser beam, thus rendering this device largely vibration insensitive. Only rotation vibration can result in a change in the output beam, though this change will only be translational (not angular), and so it will not be amplified by the lever arm of the focal length. Because the Aubin lab's dipole trap consists of two laser beams, utilizing a glass window also ensures that both beams are translated an equal distance and avoids tweaking the angle of two separate mirrors.

2.2 Snell's Law and Vertical Beam Translation

This section presents the ray optics calculations for determining the translation of the output beam from a tilted glass window.
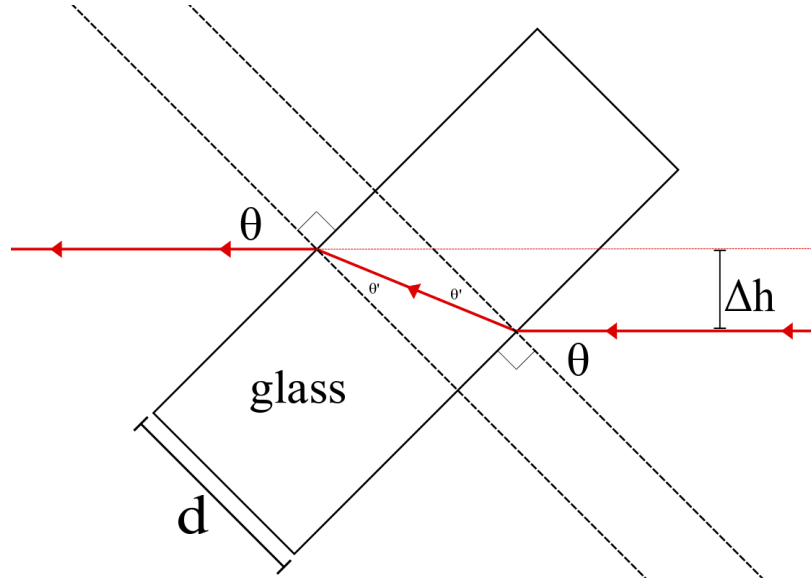
Figure 2.2: Glass window translator Using a solid glass wedge, an incident beam can be translated vertically a distance Δh as a consequence of Snell's Law. This vertical distance is dependent on the glass thickness and the relative angle of incidence (θ)

Deriving the output height relative to the incident height (Δh) requires a few nested equations related to our angle of incidence (θ). Firstly, when the beam leaves the air and enters the glass, we can derive the new angle of the beam relative to the normal of the plane of incidence using the Snell's law relationship:

$$n_{air} \cdot sin(\theta) = n_{glass} \cdot sin(\theta')$$

(2.3)

where n_{air} is the refractive index of air (reported as 1.00028), n_{glass} is the refractive index of glass (approximated as 1.5 for our initial calculations), and θ' is the new angle of the beam within the glass relative to the plane of incidence. The glass window utilized in the translator's final implementation (Thorlabs: WG12012-C Ø2" N-BK7 Broadband Precision Window, AR Coated: 1050 - 1700 nm, t = 12 mm) is reported

to have a refractive index (at room temperature) between 1.506-1.507 at 1064 nm making our initial estimate a fairly good approximation. Rearranging this equation, we find:

$$\theta' = arcsin\left(\frac{n_{air}}{n_{glass}}sin(\theta)\right) \qquad (2.4)$$

We also note that the angle θ' can be used to find the length of the hypotenuse (a) via the equation:

$$a = \frac{d}{cos(\theta')} \qquad (2.5)$$

where d is the width of the glass wedge. Drawing a line directly downwards from the red dotted line in the figure above to the point of incidence of the beam with the glass, we can create a right triangle with the beam's path through the glass as the hypotenuse. This provides the last trigonometric identity needed to solve for the change in height:

$$\Delta h = a \cdot sin(\theta - \theta') = d \cdot \frac{sin(\theta - \theta')}{cos(\theta')} \qquad (2.6)$$

This leaves us with a set of equations solely dependent on the angle of incidence.

Graphing the above equation for change in height over a range of θ equal to $-\pi/2$ to $\pi/2$ for a 1.2 cm wide glass panel yields the curve seen in Fig.2.3. The plot shows that a translation of up to 2.4 cm is possible by rotating the glass. In practice a rotation of -45 to +45 is more convenient (note the linearity in the region in Figure 2.3) yielding a translation of up to 7.9 mm. It should be emphasized that, if the faces of the glass wedge are parallel to one another, the output angle of the beam will be identical to its input angle. This conservation means that the beam translator solely acts to translate the beam vertically without further affecting the beam in any way.
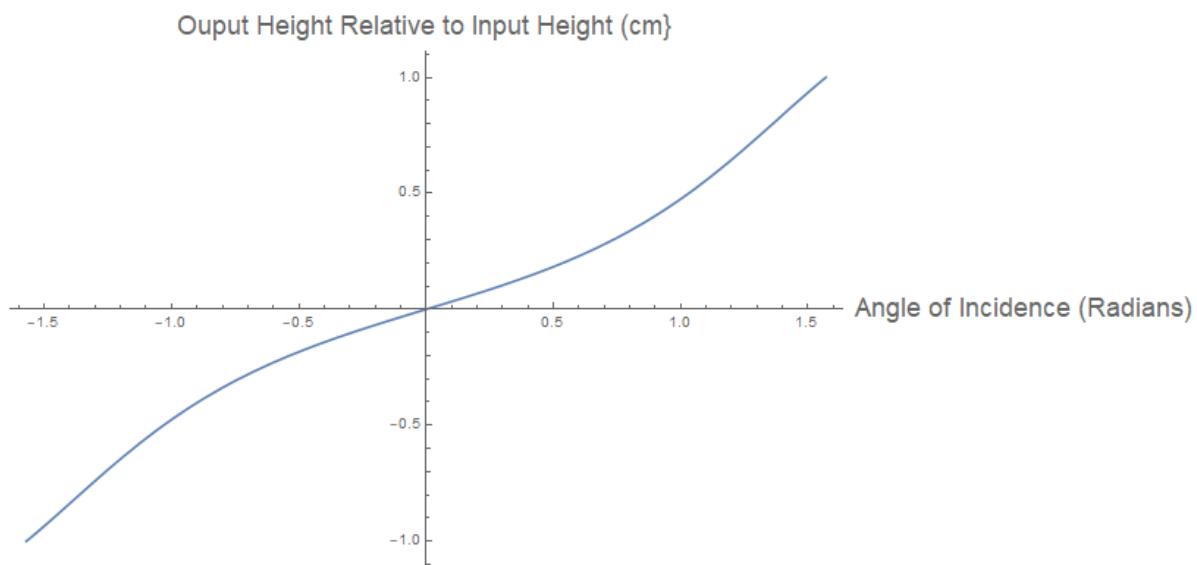
Figure 2.3: Theoretical change in beam height due to wedge rotation. By rotating the glass wedge through which our beam travels, we are able to directly control the height at which the beam exits the glass.

Chapter 3

Development of a Beam Translator

This chapter describes the work to develop an optical dipole trap translator based on a rotating glass plate. The work includes assembly of the glass plate rotational apparatus, programming the rotation controller, developing a translation trajectory, and testing its translation performance.

The rotation stage was built using a piezo motor which can rotate the glass plate smoothly and does not have any ferromagnetic parts within it. Furthermore, while the piezo motor is stationary, essentially no currents run through it. This further limits sources of magnetic fields. As the rotation stage sits close to the atom chip, any magnetic fields generated by the beam translator could be detrimental to ultracold atom experiments.

3.1 Assembly

The acquisition of a piezo motor rotating stage (Physiks Instrumente U-622 seen in Figure 3.1) and servo motor controller (Physiks Instrumente C-867 seen in Figure 3.2) had occurred prior to my being introduced to the project. A second undergraduate, Daniel Rodriguez, had begun preliminary testing involving the window prior to my arrival and had been successful in determining the accuracy and precision of the U-622 stage. He had interfaced with the servo motor using a pre-written MATLab code

13
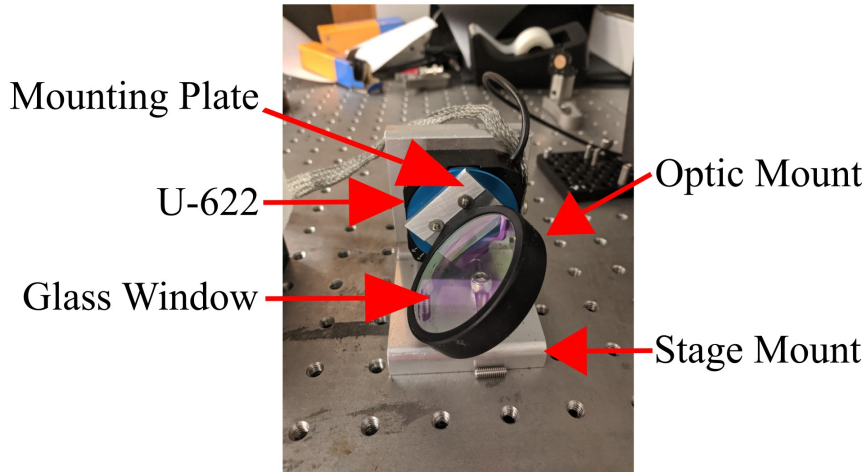
Figure 3.1: Labelled piezo motor rotating stage. The piezo motor rotating stage (U-622) is mounted to an aluminium, L-shaped stage mount. The glass window is fastened in place to the rotating face using a specially designed mounting plate and optic mount.

provided by Physiks Instrumente and had demonstrated proof of concept. However, the glass window purchased for these initial experiments included a .5 degree wedge to limit optical interference due to internal reflections (see Figure 4 in Supplementary Figures). Unfortunately, the orientation of the wedge upon installation was unclear. An important task for the glass window was to translate both incident beams an equal vertical distant so that they would continue to overlap once they were sent into the ultracold trap; misalignment on the micron-scale threatened the efficiency of the optical dipole trap and hybrid optical-magnetic trap.

My first task on the project involved assessing whether this .5 degree wedge proved harmful to the translator's function. A series of Snell's law calculations were run in Mathematica to determine the magnitude of the misalignment; a vertical difference on the order of 100 μm was deemed to be unsatisfactory for usage within the apparatus. Assuming a difference in beam path between the two translated beams of 5 cm with an overall focal length of about 50 cm following translation, the graph seen in Fig.3.3 was generated. This calculation indicated a vertical misalignment on the scale of
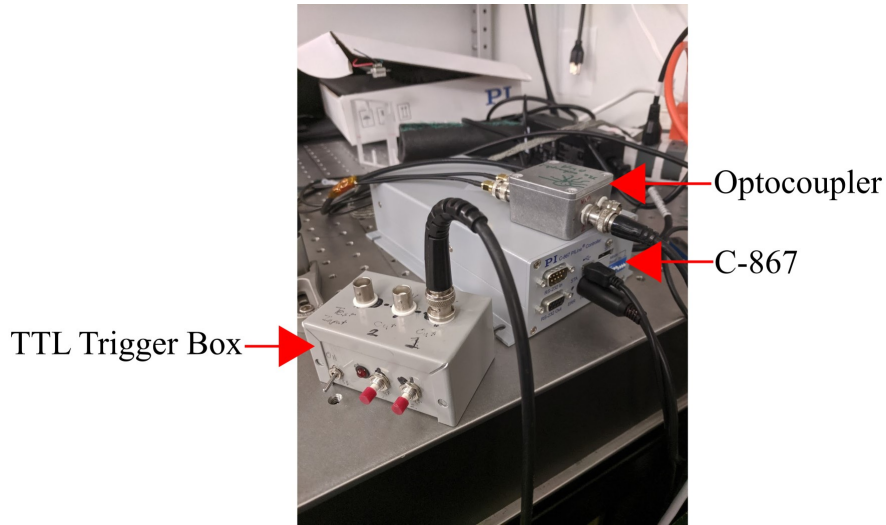
Figure 3.2: Labelled servo motor controller. A TTL trigger box was designed to output 3.3 V "high" and "low" signals for testing the apparatus. An optocoupler was constructed to avoid ground loops within the apparatus. Lastly, a C-867 piezo motor controller was purchased from Physiks Instrumente.

300 or more microns once both beams were recombined within the apparatus. As a result, a new glass window was ordered with no wedge to ensure proper functionality as well as a new optical mount. This window is a 12 mm thick, AR coated, window of fused silica two inches in diameter. An aluminium mount for attaching the optic to the U-622 was machined including a groove to restrict rotation of the optic. A new aluminium base was designed for the rotation stage to reduce the space needed to install the translator within the main apparatus (see Fig. 3.1). Furthermore, this aluminium base was machined to optimize flatness as the rotation stage requires an extremely flat mounting surface, as per the manufacturer..

3.2 Basic Testing

This new window, while specially coated to minimize internal reflections, now ran the risk of introducing interference patterns into the spatial profile of the beam. A series of tests were conducted to study the beam profile and ensure no changes occurred
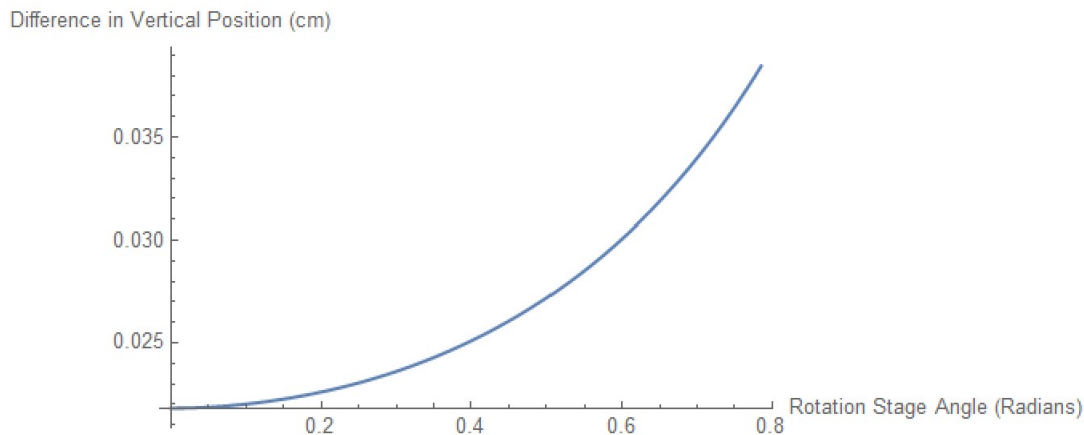
Figure 3.3: Calculated beam misalignment due to .5 degree wedge. In order to maintain atomic trapping, both trapping lasers must vertically overlap within the apparatus. The .5 degree wedge on the back of the first glass window purchased threatened to misalign the beams within the apparatus and was replaced by a flat glass window.

when rotating the glass plane from -45 to +45 degrees relative to the plane being completely vertical (see Fig.3.1 for the translator at +45 degrees). Furthermore, preliminary measurements were taken regarding the total possible vertical displacement achievable via the glass plane translator. A back-of-the-envelope calculation for vertical translation suggested ±3.5 mm as a reasonable range to vertically translate the beam relative to its initial position over the 90 degrees of rotation. My results displayed no spatial alteration in the beam as well as a total translational range of ±4.2 mm for a laser operating at 632.8 nm. It was also determined that sending beams into the translator at an angle would further minimize the chance of interference while not introducing a non-vertical translation.

3.3   Controller Automation

Satisfied with the translator's output, I next set out to automate the rotation of the stage. While I had previously controlled the stage from a PC using MATLab

code, it was necessary to design a means of signalling motion solely using TTL pulses sent into the piezo motor controller for integrating the translator into the preexisting apparatus. The Physiks Instrumente C-867 controller included software for writing macro code to upload to the U-622. Code was written to trigger the rotation stage to move using the series of 9 digital input/output (DIO) pins attached to the face of the servo controller (see Fig. 3.7). Each TTL high pulse sent into the servo would signal the window to rotate to either the 45 or -45 degree position. A 9-pin circular DIN connector (part # KMDAX-9P by Kycon) was soldered to allow the servo motor to interface with the lab's TTL generator. An optocoupler was created to separately ground the servo motor and reduce the possibility of ground loops (see Fig. 3.2).

3.4   Dynamic Testing
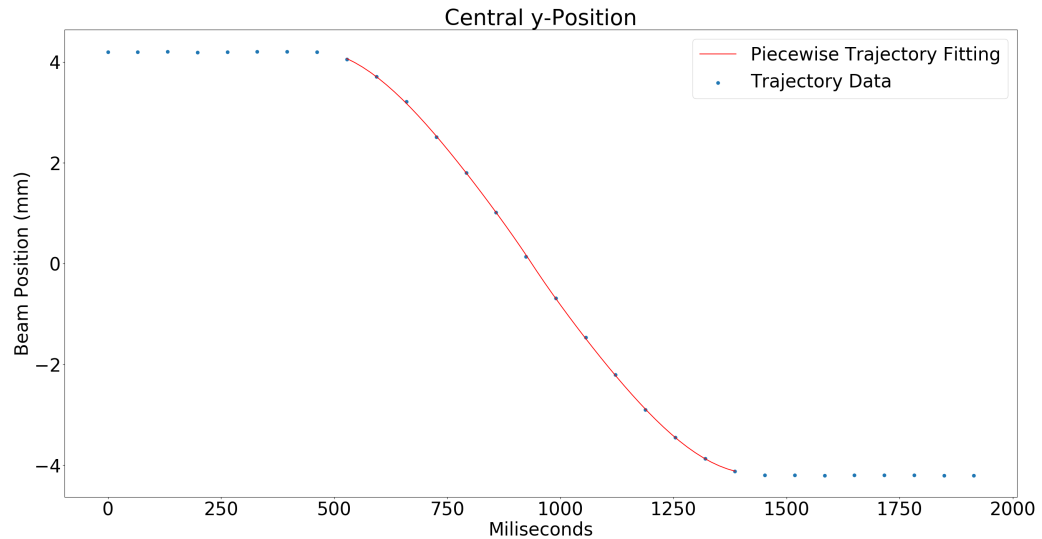
Figure 3.4: Vertical beam position vs time for the translator Error bars, while present, are too small to be visible. The piecewise trajectory function (depicted in red) matches the collected data with an R-squared value of .99997.

Due to limits in the Physiks Instrumente macro language, the rotation stage was

programmed using a step-wise acceleration function. In order to ensure an approximate total travel time of one second, the acceleration of the beam was set to 360 degrees/s^2 for the first 45 degrees of motion and -360 degrees/s^2 for the second 45 degrees of motion (see supplementary Figure 2 for graphical depictions of programmed translator parameters and their kinematic results).

A plot of vertical position of the center of the beam versus time was generated to determine whether the beam trajectory matched expectation. Using a CCD camera, a HeNe 632.8 nm laser, and neutral density filters to protect the camera from oversaturating, a series of images were collected at constant time intervals (at a rate of 15 frames per second) during beam translation (see supplementary Fig.1 for an example). The coordinates corresponding to the center of the beam were calculated for each frame of motion using a weighted average of brightness values (see the supplementary coding section for the full Python program). The vertical pixel distance travelled was remapped to match the expected vertical translation in millimeters. Plotting this data for the vertical axis versus time yielded the series of blue data points seen in Fig.3.4.

Using a least-squares regression fitting algorithm, the data was fit to the nested, piecewise function:

$$\theta = \begin{cases} \theta_i - \frac{1}{2}\alpha(t-b)^2 & t \leq a \\ \theta_i - \frac{1}{2}\alpha(a-b)^2 - \alpha(a-b)(t-a) + \frac{1}{2}\alpha(t-a)^2 & a \leq t \end{cases} \quad (3.1)$$

$$\theta' = arcsin\left(\frac{n_{air}}{n_{glass}}sin(\theta)\right) \quad (3.2)$$

$$f(\theta) = d \cdot \frac{sin(\theta - \theta')}{cos(\theta')} \quad (3.3)$$

where α, a, b, and d were fit parameters and θ_i was $\pi/4$ radians. The fit, seen in red on the graph above, produced an R-squared value of .99997 confirming the expected mathematical behavior. Furthermore, the fit angular acceleration value ($\alpha = 6.2496$

18

radians/s^2) was within .04 radians/s^2 of the expected value (6.2832 radians/s^2) and supports the assertion that the motion is symmetric. Using Savitzky-Golay filtering, velocity and acceleration profiles for the corresponding motion were also extracted (see Figure 5 and Figure 6 in Supplementary Figures).

While this data provides a strong basis for the beam translator's programmability, there are a few aspects of the motion that have yet to be validated. Firstly, the delay between when motion is requested and motion occurs must be analyzed. Secondly, the horizontal positioning of the beam appears to shift by two pixels during the beam's motion (see Figure 3 in the appendix). It is unclear if this is noise introduced from imperfections in the neutral density filters used during data collection or from the data analysis method. Lastly, the heating of atoms during motion must be verified before the beam translator can be deemed experimentally useful.

3.5   Translator Housing
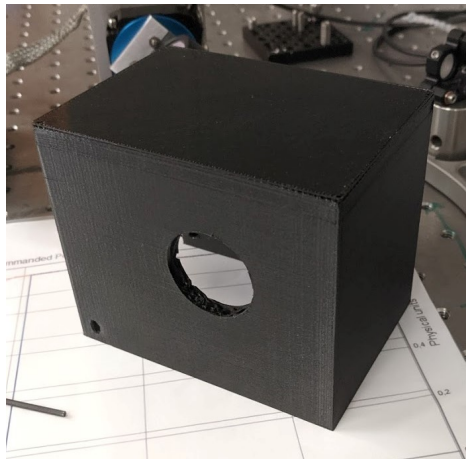
Figure 3.5: 3D printed translator box. This plastic 3D print was initially used to house the translator. However, due the high intensity beam being used for experiments, this housing was deemed inadequate and replaced with an aluminium version.

In order to ensure the safe operation of the translator a housing was developed
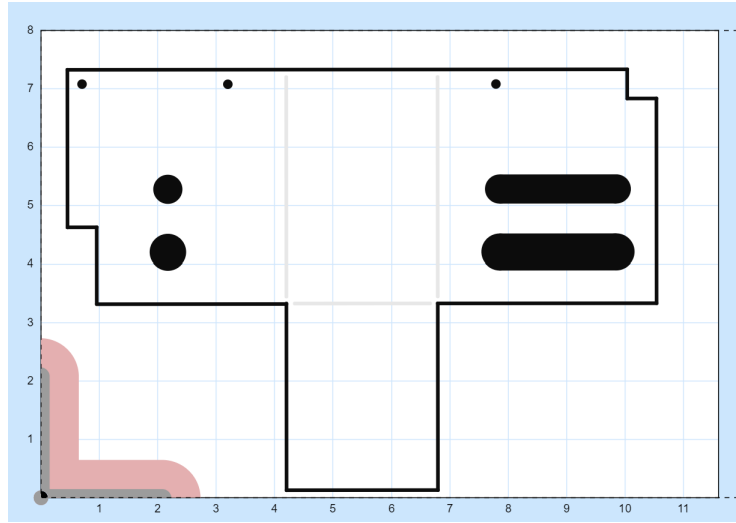
Figure 3.6: Carvey schematic for aluminium housing. While finalized, the fabrication of the new aluminium housing for the beam translator has not yet occurred. Upon reopening of the William & Mary Business School following the COVID-19 Pandemic, the box will be fully realized. Hole sizes were chosen based on the measured width of the trapping beams.

for the rotation stage. As the glass plate rotates, a small fraction of the high power 1064 nm trapping beams will reflect off of the glass. Without proper precaution, this could present a blinding and fire hazard. A series of CAD drawings were generated in Fusion 360 to 3D print a box to house the translator. However, due to the high power output of the lasers expected to utilize the translator, the plastic version of the box was discarded and planned to be replaced with an aluminium version (see Fig. 3.6). Currently, while finalized, the campus-wide lockdown has inhibited our ability to machine this model using William & Mary's Carvey located in the Business School Maker Space.

3.6   Operating the Beam Translator

Prior to any discussion of the more detailed inner-workings of the Phyisks Instrumente piezo motor, it is essential to remind the user of the fragile nature of the piezo-

mechanics within it. The user must avoid personally applying torque to the stage. Any external torque applied threatens to damage the translators rotational step size and sensors. Furthermore, any tightening or loosening of optics mounted to the rotating surface must be performed with the appropriate torque driver. See the Physiks Instrumente manual for exact specifications.

Fine-tuning the operation of the beam translator requires knowledge of the Physiks Instrumente piezo motor macro language. It should be noted that values utilized to define the kinematics of the piezo's rotation must be calculated separately and then programmed into the device; the Physiks Instrumente macro language lacks a division operation which heavily limits its ability to determine operational parameters from user-input values.

```
ROTONE  ×
SVO 1 1
FRF 1
WAC ONT? 1 = 1
RON 1 0
ACC 1 360
DEC 1 360
VEL 1 180
MVR 1 45
WAC ONT? 1 = 1
WAC DIO? 1 = 0
MVR 1 -90
WAC ONT? 1 = 1
WAC DIO? 1 = 1
WAC DIO? 1 = 0
MVR 1 90
WAC ONT? 1 = 1
WAC DIO? 1 = 1
JRC -8 DIO? 2 = 1
```

Figure 3.7: Beam translator operating macro

In order to better understand how the piezo motor functions, it helps to utilize the current macro (see Fig. 3.7) as an example. The preliminary line (*SVO 1 1*) indicates which of the piezo channels to engage. This can be thought of as turning the piezo motor on. The following line (*FRF 1*) begins a calibration protocol during which the translator rotates a full 360 degrees. Note that this calibration should be done prior to introducing any high-powered laser light. The following line (*WAC ONT? 1 = 1*) informs the piezo controller to wait until calibration is complete before moving on to the next line. This wait command (*WAC followed by some sort of boolean operation*) is used frequently within the macro to ensure that the translator fully completes the prior task before moving on to the next operation. *RON 1 0* signals the motor to return to its home position (which the piezo motor defines to be

0 degrees). Currently, this position sets the glass wedge to be entirely vertical.

Having completed start-up protocol, the program begins to define the kinematic parameters needed for the translators operation: ACC defines the positive acceleration in degrees per second, DEC defines the negative acceleration (deceleration) in degrees per second, and VEL defines the maximum magnitude allowed for the velocity. The values present in Fig. 3.7 were chosen to ensure movement from -45 to +45 degrees could be accomplished with one second of travel time. To program similar motions, begin by calculating the necessary parameters using the kinematic relationships:

$$\theta = \begin{cases} \theta_i + \frac{1}{2}at^2 & t \le \frac{\Delta t}{2} \\ \frac{\theta_f - \theta_i}{2} + \omega_{max}(t - \frac{\Delta t}{2}) + \frac{1}{2}d(t - \frac{\Delta t}{2})^2 & \frac{\Delta t}{2} \le t \le \Delta t \end{cases} \tag{3.4}$$

$$d = -a \tag{3.5}$$

$$\omega_{max} = a\frac{\Delta t}{2} \tag{3.6}$$

Here, we can exploit the need for our motion to be symmetric to set our deceleration (d) and acceleration (a) to equal and opposite values. The known parameters- initial angle (θ_i), final angle (θ_f), and duration of motion (Δt)- can then be used to solve for the unknowns: maximum rotational velocity (ω_{max}), acceleration, and deceleration. Note that all rotations performed follow the kinematic parameters previous encoded in Fig. 3.7.

Next, the MVR 1 45 command instructs the translator to rotate positive 45 degrees relative to its current position. Note that this is not an absolute motion but is strictly relative to its initial position. The wait command ensures that the full motion occurs. The following line WAC $DIO?$ $1 = 0$ instructs the translator to remain on standby until a low signal is received into DIO port 1 of the Physiks Instrumente piezo controller. It should be noted that, because of the optocoupler circuit attached to the

beam translator to ensure proper grounding, all external signals to the servo controller are reversed: TTL high signals become low signals and vice versa. The stage then rotates negative 90 degrees relative to its current position. Note that there are two *DIO* wait commands following every motion. This ensures that multiple rotations are not signalled via a single TTL pulse. This procedure defines the general algorithm: the stage waits for a TTL pulse, and, upon receiving a pulse, the rotates ± 90 degrees to the the ± 45 degree position depending on its previous location. The only other command (*JRC -8 DIO? 2 = 1*) allows the program to repeat. If DIO port two of the servo controller is high, the program jumps back in the macro eight lines earlier in the program (*WAC DIO? 1 = 0*) and runs again. As of now, DIO port two is unused which ensures the macro runs until the servo controller is turned off manually.

Due to the comparatively limited computing capacity provided by the Physiks Instrumente macro language, it seems more complicated operations may be difficult or impossible to achieve. However, currently, the vast majority of the servo controller's DIO ports are unused which could provide some adaptability. Experimenting with the DIO ports and the jump command may allow for if/then systems reminiscent of languages like Python.

Chapter 4

Development of a PID Climate Control System

4.1 PID Control

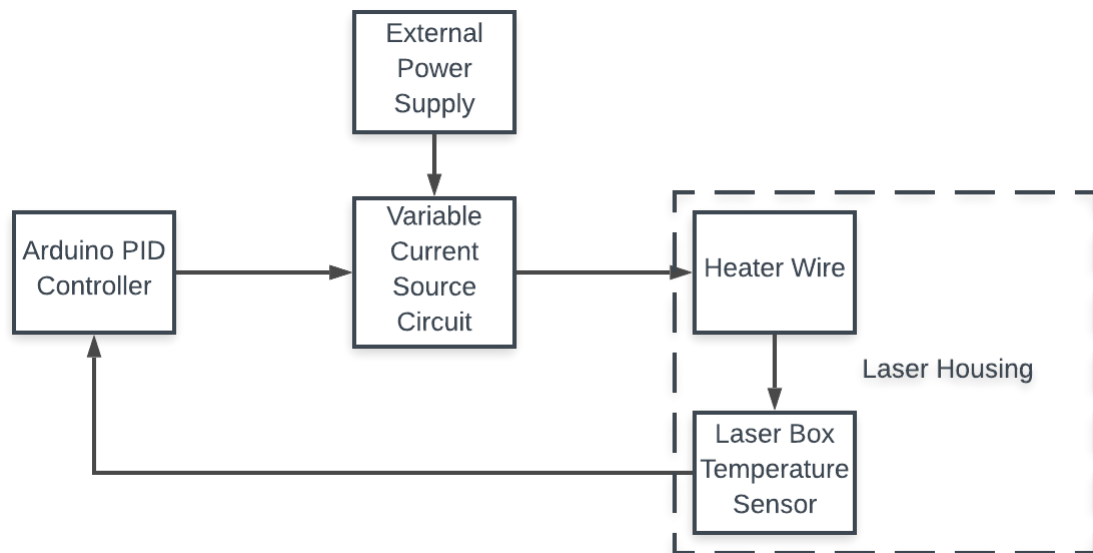Figure 4.1: PID block diagram. Here, the various elements of the PID system form a continuous feedback loop to hold the laser housing at a consistent temperature.

Overseeing nearly 97% of industrial regulatory controllers, Proportional-Integral-Derivative (PID) control systems have become the standard for managing components via electronic feedback [8]. These systems excel at holding a system variable to a user-

designated value, typically referred to as the setpoint, by responding to changes in said value over time. A PID controller determines the feedback signal necessary to hold a system at a certain value using the equation:

$$u(t) = k_p e(t) + k_i \int_0^t e(\tau) d(\tau) + k_d \frac{de}{dt} \tag{4.1}$$

where $u(t)$ is the signal from the PID controller, $e(t)$ represents the error signal or difference between the current state of the system and its setpoint ($e(t) = s - y$), and the three k values are gain parameters.

Examining this equation more closely, we can see how "PID Control" gets its name. Splitting our equation for the feedback signal into three parts, we note a term directly proportional to our error signal ($k_p e(t)$), a term reflecting the integral of our error signal ($k_i \int_0^t e(\tau) d(\tau)$), and a term based on the derivative of our error signal ($k_d \frac{de}{dt}$). By tuning the three gain constants (k_p, k_i, and k_d) multiplying the three terms, we can optimize the system to rapidly reach and then maintain the requested value. Due to the overall form of the PID equation, the correction behaves similarly to a dampened oscillation around the desired value. In most cases, the ideal implementation of a PID system aims to dampen this oscillation as rapidly as possible.

Due to their reliance on the difference between a variable's value and its setpoint, PID systems are in a constant state of error correction. This makes PID feedback systems ideal for systems designed to hold a set value for extended periods of time.

4.2   PID Climate Control Scheme

In order to thermally control the environment surrounding the lasers, the circuit seen in Fig. 4.2 was designed. Based on the difference between a reading of a temperature sensor within the laser housing and the user requested setpoint, an Arduino Due
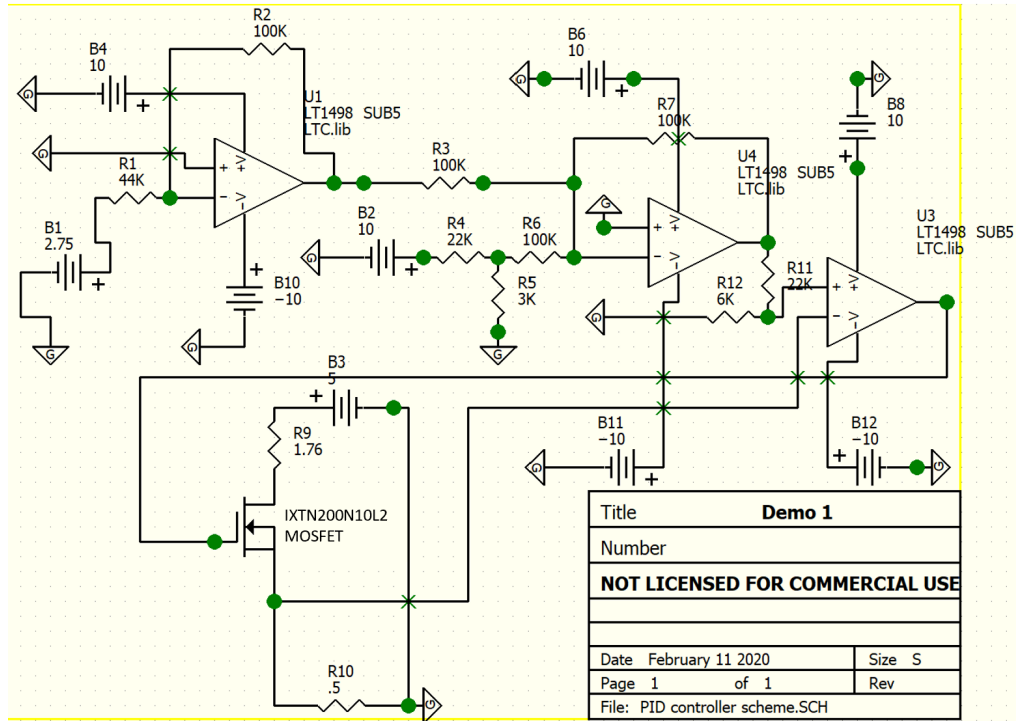
Figure 4.2: Schematic for PID MOSFET driver circuit. This circuit shifts the analog voltage output by an Arduino Due into a proper voltage range for use as the gate voltage of a MOSFET. This MOSFET is then used as a tunable resistor in a variable current source.

outputs a PID correction signal using its analog voltage port. The Arduino Due can only output 0.55-2.75 V using this port. As a result, a series of LT1498 operational amplifiers are used to set the minimum correction signal value to 0 V and to amplify the maximum output to 5 V. This correction signal is then used as the gate voltage to an IXTN200N10L2 high power MOSFET as part of a variable current source. In this case, the load resistor for our current source is a series of loops of copper wire wound around the laser housing. The wire radiates heat proportional to the square of the current fed through it thereby raising the temperature of the housing. As a result, by controlling the gate voltage using a PID system, the current and connected heating can be controlled. Simulations of the circuit run using 5Spice indicated that the Arduino Due's analog voltage could be mapped to a current range of 0.003-2.175

A.

A setpoint of 25ºC was decided upon for the system. An aluminium-coated laser housing roughly two cubic feet in size was created to serve as a climate-controllable environment. This housing also served to reduce the effect of air currents on the laser temperature. Several loops of copper wire was wrapped around the aluminium housing to serve as the heating element. In order to avoid inducing unwanted magnetic fields inside of the laser housing, the copper wire was twisted into a helical shape thereby creating multi-directional current flow. The PID current source circuit was assembled and soldered prior to the removal of students from William & Mary's campus due to the COVID-19 pandemic. While initial testing of the circuit proved satisfactory, data has yet to be collected for the system.

4.3   PID Schematic: In-Depth Look

In examining Fig. 4.2, the circuit schematic can be broken down into three distinct subcircuits (seen outlined in Fig. 4.3). Beginning with the red section, the Arduino Due (the 2.75 V source labelled B1) is sent through an inverting amplifier. This adjusts the magnitude of the Arduino's .55-2.75 V range to a negative 1.25-6.25 V range. This signal is then sent to the green section. This voltage adder inverts the signal once again and adjusts the previous voltage range by 1.25 V; our negative 1.25-6.25 V range leaves the green section as a positive 0-5 V range. Having corrected our voltage range, we now have the proper voltage to operate our current source.

Both blue areas serve the same purpose: creating a variable current source. The voltage range from the previous portions is fed into the non-inverting port of the operational amplifier while the inverting port is connected after the MOSFET in our current loop. The output of this operational amplifier is then connected to the gate of the MOSFET. In order to try to equalize the voltage between both ports, the
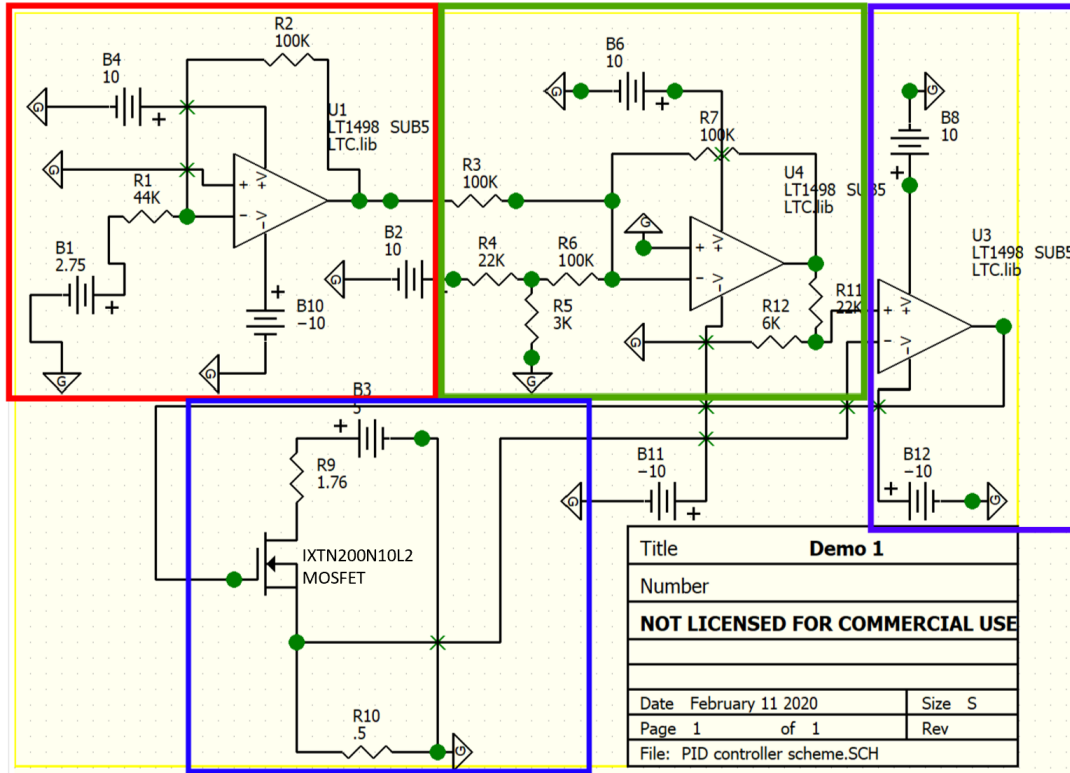
Figure 4.3: PID control circuit broken down into subcircuits. Red: Inverting amplifier. Green: Inverting voltage adder. Blue: Variable current source.

resistance of the MOSFET is adjusted. A higher voltage from the Arduino requires the MOSFET to have lower resistance. This variable resistance in the loop then leads to variable required current depending on the voltage drop across the MOSFET as a result of Ohm's Law.

Here, our radiated heat for controlling the temperature of the laser housing is proportional to the current through the wire. By including a temperature sensor within the laser housing, the voltage output generated by our Arduino can be adjusted based on the difference between the measured and requested values. This then tunes the magnitude of current through the wire leading to a programmable feedback system.

Closed-Loop Response	Rise Time	Overshoot	Settling Time	Steady-State Error	Stability
Increasing K_P	Decrease	Increase	Small Increase	Decrease	Degrade
Increasing K_I	Small Decrease	Increase	Increase	Large Decrease	Degrade
Increasing K_D	Small Decrease	Decrease	Decrease	Minor Change	Improve

Figure 4.4: Effects of independently adjusting PID gain tuning parameters. While somewhat reductive, this table provides some guidance for the manual tuning of the PID gain parameters k_p, k_i, and k_d. Taken from Ang et al, *PID Control System Analysis, Design, and Technology* (2005).

4.4 PID Gain Parameter Tuning

While adequate for initial testing, the current gain parameters (k_p, k_i, and k_d in the error signal equation) programmed into the Arduino Due may require adjustment. Unfortunately, much of the process of identifying the optimal values for these parameters is an art rather than a science. This is exacerbated by the system itself requiring a particularly long warming period. Utilizing the Arduino Due's plotting functionality somewhat automates the process. For guidance on manually tuning, Fig.4.4 offers a useful guide for the effects of independently adjusting each value.
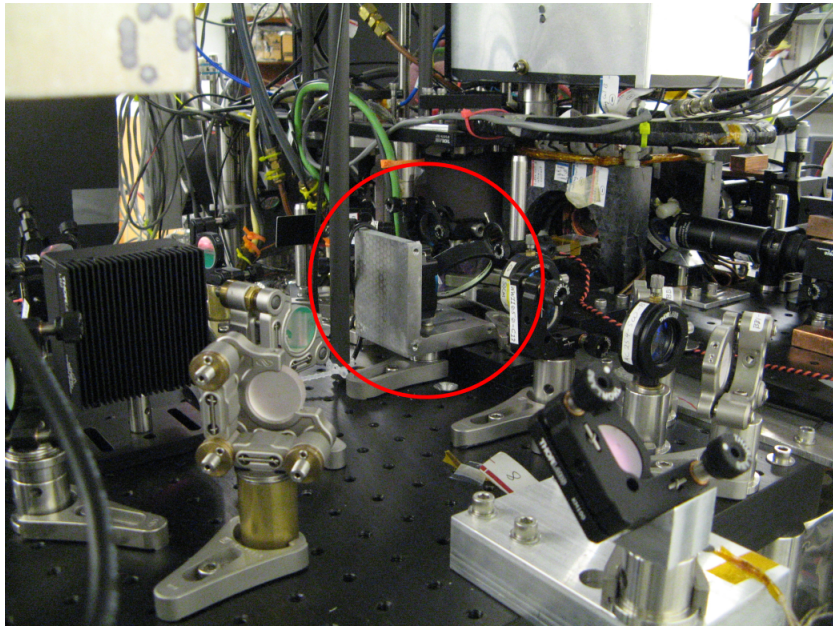
Chapter 5

Outlook

Figure 5.1: Installed beam translator. The beam translator (circled in red) currently installed into the Aubin Lab ultracold apparatus. The beam translator is set for testing following the lowering of laboratory restrictions.

While unfortunately stalled due to the COVID-19 pandemic, both the vertical beam translator for the Aubin Lab's optical dipole trap and the PID control system for maintaining optimal housing temperature for the lab's lasers are in their final testing stages. Upon their completion, each should open up new possibilities for experimentation and data collection. For the beam translator, the additional capability

to easily manipulate atoms within the ultracold apparatus is expected to greatly reduce atomic losses during experiments involving the microwave atom chip. Similarly, the temperature control system will allow for reductions in noise as well as an overall increase in the lifespan of the lab's equipment.

5.1   Finalizing the Beam Translator

In its current state, the beam translator is functional but needs to be verified and optimized for the ultracold apparatus. In particular, while the translator's rotation was programmed to minimize jerk as much as possible, the heating of the atoms within the apparatus following motion has yet to be quantified. Should the atomic losses from the trap be particularly noticeable following translation, the rotation macro will need to be reworked. Possibilities for mitigating these losses include lowering the acceleration parameters thereby increasing travel duration or reworking the central kinematic equation. Furthermore, once experiments with the microwave atom chip begin, the translational distances may need to be readjusted or the order in which events in the macro occur may need to change.

Hopefully, the aforementioned Carvey schematic should properly house the translator. However, in the case that it does not, the model may need to be adjusted. In particular, the windows of the housing may need to be widened or readjusted should the layout of the beam path be changed.

5.2   Finalizing the PID System

The PID system has been tested on a small scale model of the laser housing, but full quantitative analysis has yet to be performed. Furthermore, while the majority of the circuit is currently powered via a wall wart, the Arduino Due still requires USB power from a computer. While the USB will be required for collecting preliminary

data during testing, the goal is to have the system powered entirely by a wall wart. Also, the circuitry needs to be properly house and heatsunk to be usable. While not yet measured, the IXTN200N10L2 MOSFET releases a considerable amount of heat. Unless given an outlet, this could prove dangerous during the long-term usage of the system. This is particularly salient considering that the PID system is meant to be activated and then left on, possibly indefinitely.

Chapter 6

Appendix

Supplementary Code

Python Code for Calculating Central Position of Gaussian Beam

This program takes a series of greyscale .tif or .png files with gaussian beam profiles as input (see Fig.1 for an example). For each image, the program calculates the center of the beam using a weighted average of the x,y-intensity values. For our purposes, these centers were plotted with respect to imaging time.

```python
import os
import matplotlib.pyplot as plt
from numpy import linspace, std
from scipy.optimize import curve_fit
from PIL import Image
plt.rcParams.update({'font.size':34})
plt.rc('axes',labelsize=34)

"""Arrays for housing data"""
xcenters=[]
ycenters=[]
files=[]
time=50 #ms
times=[]

"""Data Processing"""
for filename in os.listdir(r'C:\Users\Bennett\Desktop\pics2'):
    name=str(filename)
```

```python
19      if name.endswith(".png")==True:
20          files.append(int(name.rstrip('.png')))
21      if name.endswith(".tif")==True:
22          files.append(int(name.rstrip('.tif')))
23      print("Finding value for: ", str(filename))
24      im=Image.open(r'C:\Users\Bennett\Desktop\pics2\{}'.format(filename))
25      xmin,ytop,xmax,ybot=im.getbbox()
26      xweight=0
27      yweight=0
28      totweight=0
29
30      """Calculating weighted values for each pixel"""
31      for i in range(xmin,xmax):
32          for j in range(ytop,ybot):
33              weight=im.getpixel((i,j))
34              if weight<20:
35                  pass
36              else:
37                  xweight+=i*weight
38                  yweight+=j*weight
39                  totweight+=weight
40      xcenter=xweight/totweight
41      ycenter=yweight/totweight
42      xcenters.append(xcenter)
43      ycenters.append(ycenter)
44  times=[time*x for x in files]
45
46  """Fitting the Data"""
47  stimes=[]
48  scenters=[]
49  for item in times:
50      stimes.append(item)
51  for item in ycenters:
52      scenters.append(item)
53  stimes.sort()
54  scenters.sort(reverse=True)
55  start=stimes.index(350)
56  end=stimes.index(1100)
57  shorttimes=[]
58  shortcenters=[]
59  for i in range(start,end+1):
60      shorttimes.append(stimes[i])
61      shortcenters.append(scenters[i])
62
63  def theta(t,a,b,c):
```

```
64      return numpy.piecewise(t,[t<a,a<=t],[lambda t: (numpy.pi/4)-.5*(2*c/(1000**2))\\
65      *(t-b)**2, lambda t: (numpy.pi/4)-.5*(2*c/(1000**2))*(a-b)**2- \\
66      (2*c/(1000**2))*(a-b)*(t-a)+.5*(2*c/(1000**2)*(t-a)**2])
67  def theta_prime(t,a,b,c):
68      return numpy.arcsin((1/1.5)*numpy.sin(theta(t,a,b,c)))
69  def h(t,a,b,c,d,e):
70      return c+d*numpy.sin(theta(t,a,b,e)-theta_prime(t,a,b,e))\\
71      /numpy.cos(theta_prime(t,a,b,e))
72  popt, pcov=curve_fit(h, shorttimes, shortcenters, p0=[600,310,300,1900,3.14],\\
73      bounds=([500,250,200,0,3],[900,400,740,2000,10]))
74  xs=numpy.linspace(400,1050)
75  residuals=shortcenters-h(shorttimes,*popt)
76  ss_res=numpy.sum(residuals**2)
77  ss_tot=numpy.sum((shortcenters-numpy.mean(shortcenters))**2)
78  r_squared=1-(ss_res/ss_tot)
79  #def func(t,a,b,c,d):
80      #return a+(b-a)*(10*((t-d)/c)**3-15*((t-d)/c)**4+6*((t-d)/c)**5)
81  """ Plotting the Data"""
82  plt.figure(1)
83  plt.scatter(times,xcenters)
84  plt.xlabel("Miliseconds")
85  plt.ylabel("Pixel Position")
86  plt.title("Central x-Position")
87  plt.figure(2)
88  plt.scatter(times,ycenters, label="Trajectory Data")
89  plt.errorbar(times,ycenters,yerr=0.39646, xerr=None, fmt='none')
90  plt.plot(xs,h(xs,*popt),color='r',label="Piecewise Trajectory Fitting")
91  plt.xlabel("Miliseconds")
92  plt.ylabel("Pixel Position")
93  plt.title("Central y-Position")
94  plt.legend()
95  plt.show()
96
```

Supplementary Figures

Figure 1: IR image of laser beam profile. Images were compiled to determine the vertical position of the beam versus time when using the rotation macro.
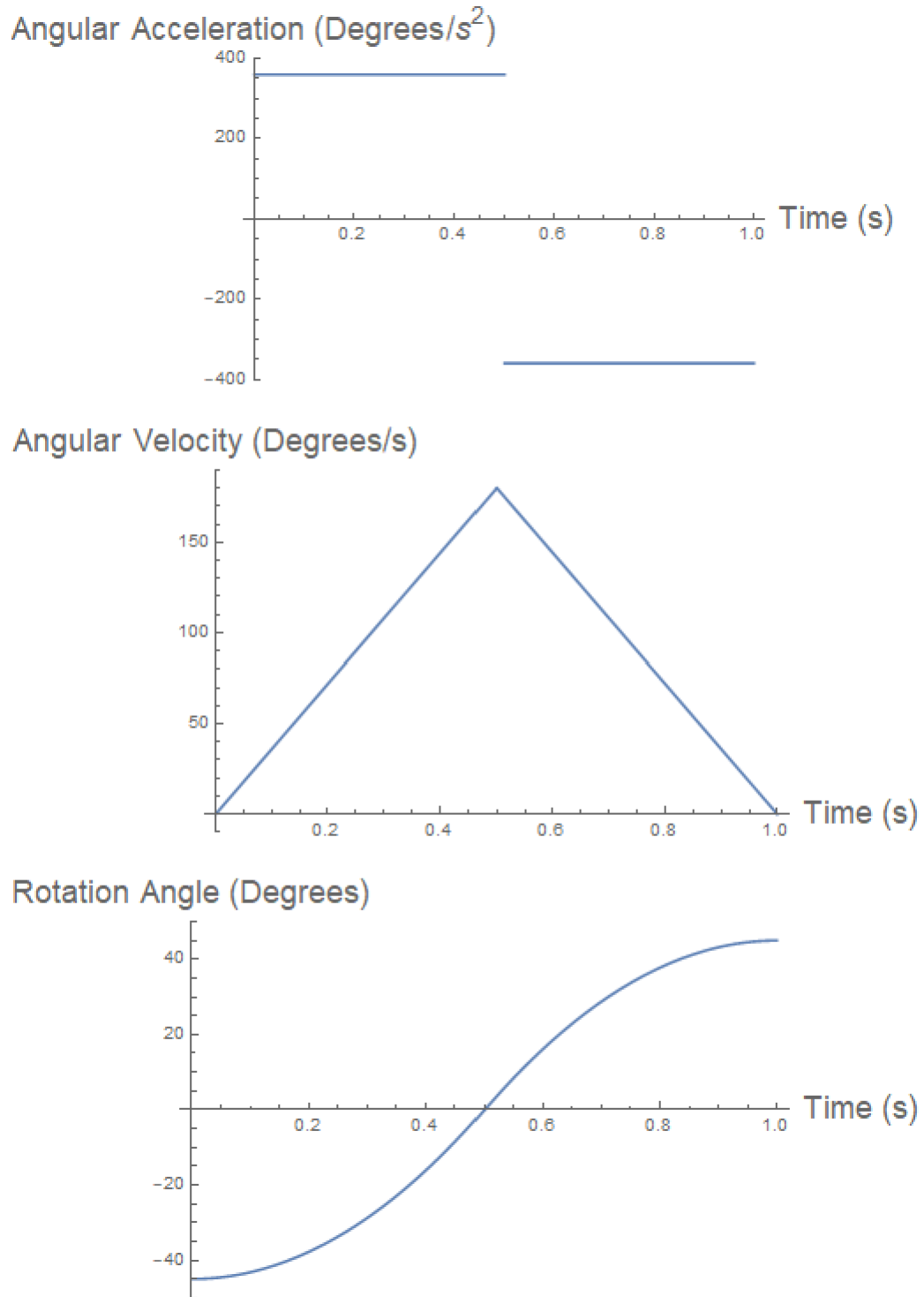
Figure 2: Programmed kinematic equations for rotation stage. Top: angular acceleration versus time. Middle: angular velocity versus time. Bottom: rotation angle versus time.
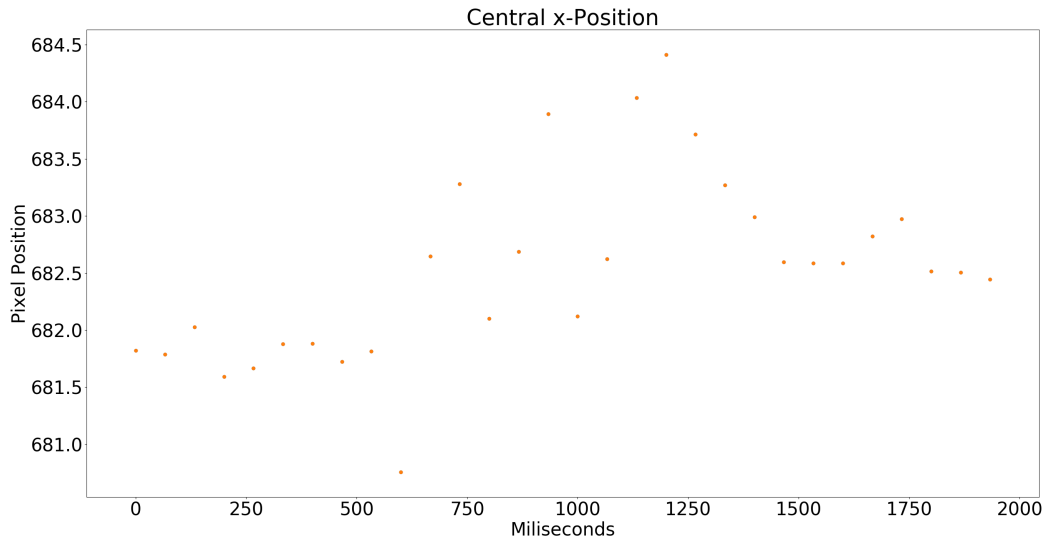
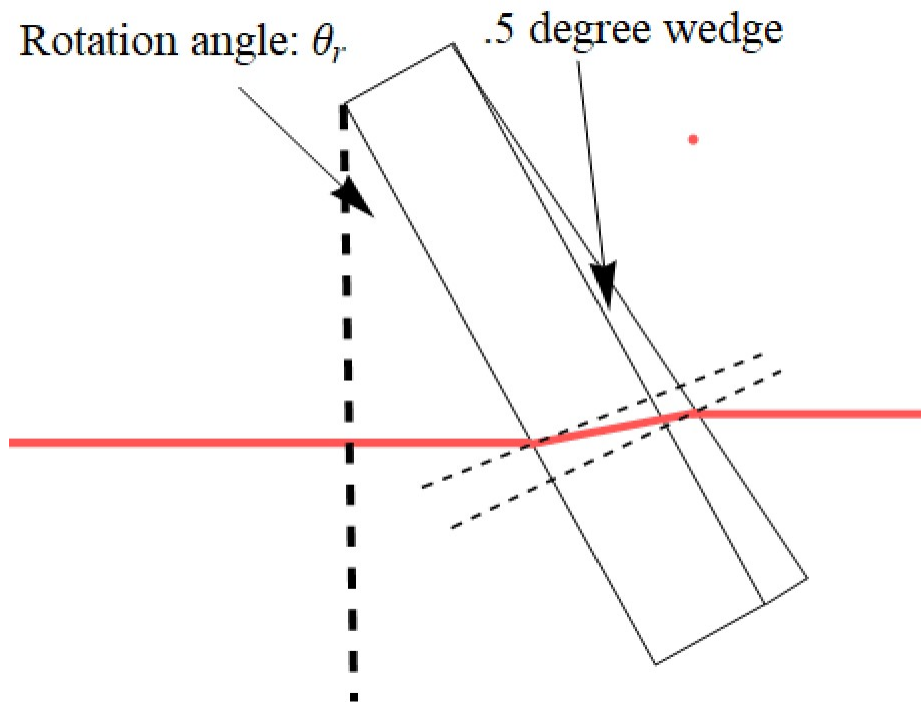Figure 3: Graph of central x-position versus time for beam translator motion

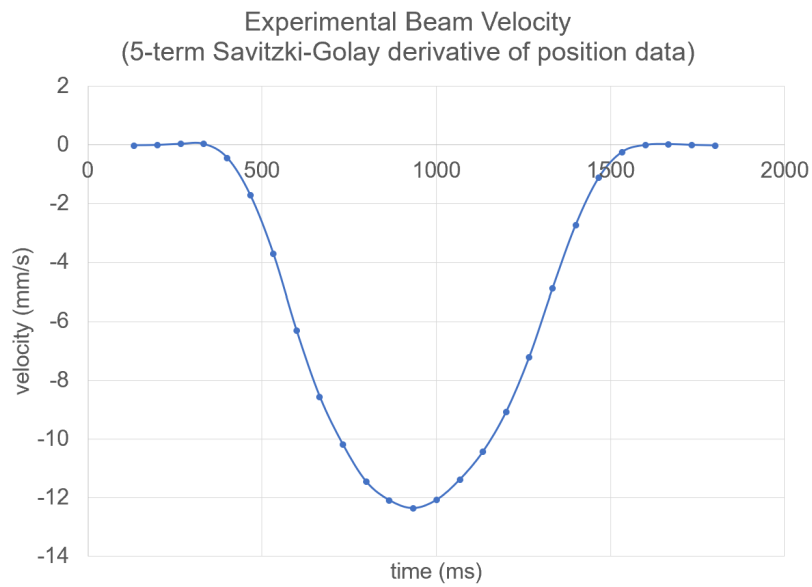Figure 4: .5 degree wedge glass window

Figure 5: 5-term Savitzky-Golay velocity extracted from beam translator data.
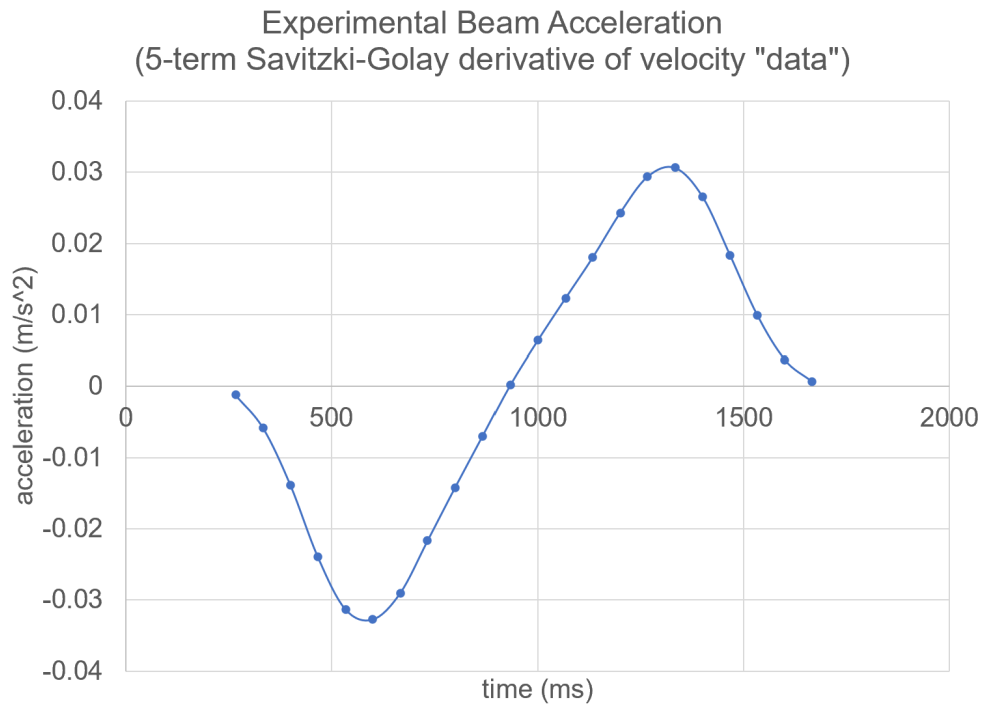Peak velocity=-12.35 mm/s

Figure 6: 5-term Savitzky-Golay acceleration extracted from beam translator data.
Peak acceleration=± 0.03 m/s^2

.

Bibliography

[1] Raab, E.L et al. "Trapping of Sodium Atoms with Radiation Pressure". *Physical Review Letters*, vol.59, no.23, 1987. pp.2631-2634

[2] Chandler, David. "Ultracold Molecules Hold Promise for Quantum Computing". *MIT News*, 2017. http://news.mit.edu/2017/ultracold-molecules-hold-promise-quantum-computing-qubit-0727

[3] Fancher et al. "Microwave AC Zeeman Force for Ultracold Atoms". *Physical Review A*, vol 97, 2018. pp.043430

[4] Ospelkaus et al, "Microwave Quantum Logic Gates for Trapped Ions". *Nature*, vol. 476, 2011. pp.181-184

[5] Kishimoto et al, "Direct Evaporative Cooling of Potassium 41 into a Bose-Einstein Condensate". *Physical Review Letters A*, vol 79, 2009. pp.031602

[6] Thalhammer et al, "Double Species Bose-Einstein Condensate with Tunable Interspecies Interactions". *Physical Review Letters*, vol 100, pp.210402

[7] Grimm et al, "Optical Dipole Traps for Neutral Atoms". *arXiv*, 1999. https://arxiv.org/abs/physics/9902072

[8] Desborough et al, "Increasing Customer Value of Industrial Control Performance Monitoring", *Honeywell Hi-Spec Solutions*, 2002.

[9] Pritchard et al, "Cooling Neutral Atoms in a Magnetic Trap for Precision Spectroscopy". *Physical Review Letters*, vol 51, 1983. pp.1336-1339

[10] Pritchard et al, "Light Traps Using Spontaneous Forces", *Physical Review Letters*, vol 57, 1986. pp.310-313

[11] A. Burchianti et al, "Dual-species Bose-Einstein Condensate of 41K and 87Rb in a Hybrid Trap", *Physical Review A*, vol 98, 2018. pp.063616

[12] S. Chu et al, " Trapping of Neutral Sodium Atoms with Radiation Pressure", *Physical Review Letters*, vol 59, 1987. pp.2631-2634

[13] M. Inguscio et al, "Bose-Einstein Condensation of Potassium Atoms by Sympathetic Cooling", *Science*, vol 294, 2001. pp 1320-1322

[14] "Cold Atom Laboratory." NASA, NASA, coldatomlab.jpl.nasa.gov/.

[15] C. Chin, R. Grimm, P. Julienne, and E. Tiesinga, "Feshbach resonances in ultracold gases", *Rev. Mod. Phys.*, vol 82, 2010. pp.1225-1286